Weight-Transducerless Rollback Mitigation Adopting Enhanced MPC With Extended State Observer for Direct-Drive Elevators

Gaolin Wang, *Member, IEEE*, Ying Wang, Jin Xu, Nannan Zhao, and Dianguo Xu, *Senior Member, IEEE*

***Abstract*—The permanent magnet traction machine has become the tendency of modern gearless elevators, because of small volume, high efficiency, and good dynamics. However, the direct-drive elevator car will slide during the electromagnetic brake releasing at elevator startup, if the speed controller cannot generate a suitable electromagnetic torque to trace the change of the uncertain disturbance on traction sheave. To attenuate the car sliding of the gearless elevator installed with an ordinary resolution encoder, a weight-transducerless rollback mitigation strategy adopting an enhanced model predictive control with extended state observer (ESO) for speed loop is proposed. The ESO is used to overcome the mismatch of predictive model caused by the braking torque and the unknown car load. Both the stability and the parameter selection of the observer are analyzed. Additionally, a nonlinear tracking differentiator is used to process the raw speed signal generated by the conventional speed differential sampling instead of the low-pass filter, which can overcome the vibration of the elevator car when the brake releases. Finally, experimental results verify that the proposed control strategy can achieve shorter sliding distance and smaller sliding speed for the direct-drive elevator installed with an ordinary-resolution encoder.**

***Index Terms*—Extended state observer (ESO), gearless elevator, model predictive control (MPC), nonlinear tracking differentiator (NTD), riding comfort, rollback mitigation, weight transducerless.**

I. Introduction

As the efficient and convenient tools of vertical transport, elevators are significant for modern buildings. Therefore, new technologies for an elevator drive system have been developed increasingly [1], [2]. Modern architecture requires that the traction machine driving elevators should have special characteristics, such as small volume, high efficiency, and high dynamic performance. Conventional traction machines with worm gear transmission cannot meet these requirements. In order to improve the performance of elevators, gearless permanent magnet traction machines have been developed quickly [3]–[6]. Meanwhile, the control system of direct-drive permanent magnet traction machines also encounters many challenges. When the elevator operates from standby mode to the running mode, restricted by the dynamics of the conventional control algorithm, and the unknown disturbance exerted on the elevator sheave, the electromagnetic torque is difficult to keep up with the change of the external uncertain disturbance. Thus, the torque exerted on the sheave cannot be balanced, which causes sliding and seriously impacts on the riding comfort of passengers.

Conventionally, the load torque is usually measured by weight transducers installed at the bottom of the elevator car. However, the feedforward compensation has some disadvantages. The colinearity of the car load and the distortion of antivibration rubber will degrade when the usage time of weight transducer becomes longer. In addition, weight transducers will not only reduce the system robustness, but also increase the cost. Therefore, the weight-transducerless control is an emerging technique for the gearless elevator traction machine drives.

Various advanced control strategies have been proposed to optimize the speed control performance and enhance the robustness against unknown disturbance [7]–[11]. However, the weight-transducerless control for an antirollback of elevator car should consider special requirements of riding comfort. Recently, some novel solutions have been proposed [12]–[16]. In [12], through evaluating the rate of change of speed by the quadratic error comparison, the load torque can be calculated accurately according to the established mechanical model. In [13], a novel torque control strategy based on the friction model of a traction system was described as a searching logic. In [14], the load torque was traced by the compensation torque calculated by dichotomy and staircase algorithms, respectively. However, mechanical vibration is difficult to be avoided due to the sudden change of torque reference. In [15], an accurate speed measurement method for Sin–Cos encoder was introduced, and a feedforward compensation strategy adopting load torque observer was proposed to improve the performance of elevators. In [16], an adaptive torque compensation strategy based on fuzzy self-tuning of the rate of change of electromagnetic torque was proposed, and the accurate subdivided position information based on Sin–Cos encoder is needed. However, for the elevator installed with an ordinary resolution encoder, the performance of this control strategy will deteriorate.

Therefore, the weight-transducerless starting torque control strategy using ordinary resolution encoders become a key technique of modern elevator applications. This kind of control strategy should have the function of rollback mitigation, which means that it can provide a smooth startup with little sliding distance and acceptable mechanical vibration. Since the rollback

Manuscript received February 1, 2015; revised July 23, 2015; accepted August 27, 2015. Date of publication September 1, 2015; date of current version January 7, 2016. This work was supported in part by the Research Fund for the National Science Foundation of China (51207030, 51522701), and the Power Electronics Science and Education Development Program of Delta Environmental and Educational Foundation (DREK2015002). Recommended for publication by Associate Editor A. Muetze.

The authors are with the School of Electrical Engineering and Automation, Harbin Institute of Technology, Harbin 150001, China (e-mail: WGL818@hit.edu.cn).

Color versions of one or more of the figures in this paper are available online at http://ieeexplore.ieee.org.

Digital Object Identifier 10.1109/TPEL.2015.2475599

mitigation control should be accomplished in a very short time to balance the uncertain and nonlinear load torque, the preferred control method should have a good dynamic performance. Model predictive control (MPC) can get a faster response by adjusting parameters of the trajectory function. In addition, MPC also has advantages, such as small overshoot and high control accuracy. It has been successfully applied in motor drives, power converters, and other industry applications [17]–[21]. Considering the characteristics of MPC, it can be a potential approach for antirollback control of weight-transducerless elevators.

However, the conventional MPC speed controller is difficult to achieve high-performance control of the elevator starting torque. During the brake releasing, the near-zero speed is difficult to be calculated from an ordinary resolution encoder, and the uncertain disturbance caused by the nonlinear change of braking torque will lead to the mismatch of a predictive model. This kind of model mismatch will cause an inaccurate prediction and speed error at the steady state. The active disturbance rejection control (ADRC) can attribute the uncertainty factors of the plant to unknown disturbance which can be calculated. Nowadays, ADRC has been successfully applied in power electronics and electrical drives [22]–[24]. ADRC mainly consists of the nonlinear tracking differentiator (NTD), the extended state observer (ESO), and the regulating law. ESO has excellent dynamic performance, which can quickly trace the change of unknown disturbance without accurate mathematical disturbance model, and NTD can effectively extract continuous signal and differential signal from noncontinuous input signal [25], [26]. Therefore, the combination of advantages of ADRC and MPC can achieve high-performance control of direct-drive elevators.

In this paper, a novel rollback mitigation control strategy adopting enhanced MPC with an ESO and a NTD is proposed to enhance the riding comfort of the weight-transducerless elevator installed with an ordinary resolution encoder, and the proposed method can improve the dynamic and steady performance without requiring the weight information of passengers during the brake releasing process. The torque current reference can trace the uncertain load more quickly because of the speed MPC involved. Additionally, the ESO can eliminate the steady-state speed error caused by the conventional speed MPC strategy, which is critical for antirollback control of weight-transducerless elevator drive. Especially, the accurate speed feedback can be acquired from the NTD to enhance the rollback mitigation. The external disturbance information obtained by the ESO is added into the predictive model to match the model in each sampling period.

This paper proceeds as follows. First, a dynamic model of the elevator traction system is described in Section II to illuminate the technical difficulties of the rollback mitigation without using a weight transducer. Second, the enhanced MPC strategy for rollback mitigation is established in Section III. In addition, the stability and the parameter selection of observer are investigated. Finally, in Section IV, the proposed control strategy is verified by experimental comparisons.

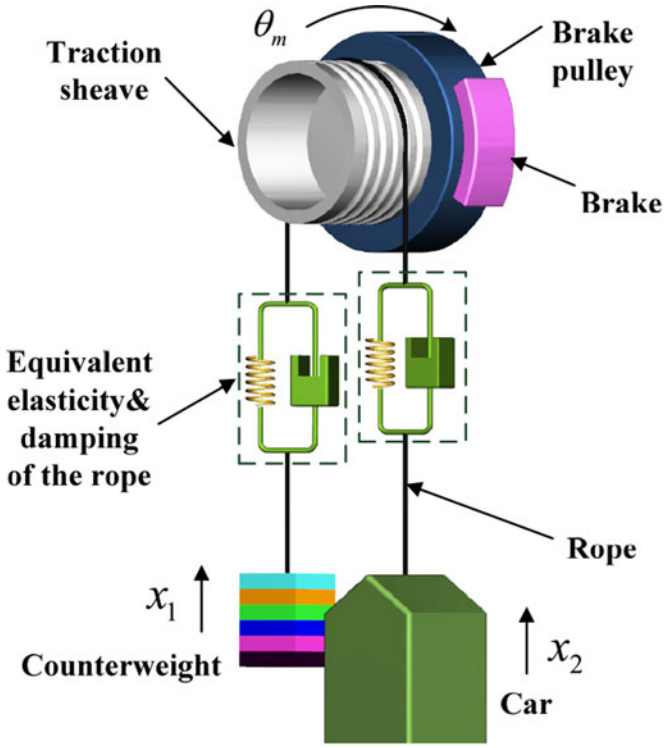

Fig. 1. Equivalent model of the direct-drive elevator traction system.

II. Dynamic Model of the Elevator Traction System

The drive system, the car, and the counterweight are the main parts of the gearless elevator. An electromagnetic brake mounted on the brake pulley is used to hold the rotor at standstill when the elevator converts to standby mode. The dynamic model of direct-drive elevator is established ignoring the effects of the compensation wheel, weight compensation ropes, and friction damper. As a result, the equivalent model is shown in Fig. 1. Taking the rigidity coefficient and the damping coefficient of the traction rope into consideration, the dynamic model of the traction system can be described as follows:

$$\begin{cases} M_1\ddot{x}_1 - k_1(-\theta_m R_m - x_1) + M_1 g - b_1(-\dot{\theta}_m R_m - \dot{x}_1) = 0 \\ M_2\ddot{x}_2 - k_2(\theta_m R_m - x_2) + M_2 g - b_2(\dot{\theta}_m R_m - \dot{x}_2) = 0 \\ J\ddot{\theta}_m + R_m k_2(\theta_m R_m - x_2) - R_m k_1(-\theta_m R_m - x_1) \\ \quad + R_m b_2(\dot{\theta}_m R_m - \dot{x}_2) - R_m b_1(-\dot{\theta}_m R_m - \dot{x}_1) = T_e \end{cases} \tag{1}$$

where k_1 and b_1 are the stiffness coefficient and the damping coefficient of the rope on counterweight side, M_1 is the mass of the counterweight, x_1 is the counterweight displacement, g is the coefficient of gravity acceleration, k_2 and b_2 are the stiffness coefficient and the damping coefficient of the rope on car side, M_2 is the mass of the car, x_2 is the car displacement, θ_m is the mechanical position of the traction motor, J is the total inertia of the traction system, R_m is the radius, and T_e is the electromagnetic torque generated by the traction machine.

The relationship between the friction force f and the mechanical velocity v_m can be expressed as follows, which can make it

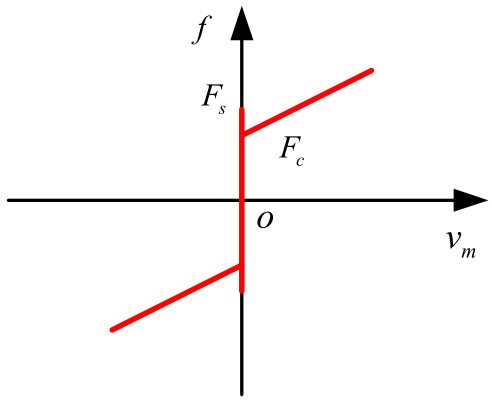

Fig. 2. Friction model of traction sheave.

easier to analyze the friction torque characteristics:

$$f=\begin{cases} F_l, & \text{if} \quad v_m=0 \quad \text{and} \quad |F_l|<F_s \\ F_s\text{sign}(F_l), & \text{if} \quad v_m=0 \quad \text{and} \quad |F_l|\geq F_s \\ F_c\text{sign}(v_m)+\sigma v_m, & \text{if} \quad v_m\neq 0 \end{cases} \tag{2}$$

where F_l is the force generated from external parts, F_c is the coulomb friction, σ is the coefficient of viscosity, and F_s is the maximum static friction force.

When the brake releases completely, according to the friction model in (2), the torque judgement that drives the traction machine from standstill to the rotating state is

$$|F_e-(M_2-M_1)g|>F_s \tag{3}$$

where F_e is the force generated by the traction machine, and the judgement that makes the traction machine convert from the rotating state to standstill is

$$|F_e-(M_2-M_1)g|<F_c. \tag{4}$$

It can be concluded that the force generated by the traction machine to maintain the car at standstill is not a fixed but variable value. To be specific, the model of friction is shown in Fig. 2.

According to the friction model, the electromagnetic torque to maintain the traction sheave at standstill is a range. It is difficult to accurately calculate the electromagnetic torque to balance the equivalent load torque from the mathematical model when taking the nonlinear characteristic of the mechanical brake releasing into consideration. Therefore, those methods calculating the compensation torque depended on accurate mechanical models cannot achieve good robustness in the startup control of direct-drive elevators.

During the elevator startup, the conventional PI controller used as speed regulator can hardly meet the requirements of small mechanical vibration and fast adjustment at the same time when using the ordinary incremental encoder. However, this kind of encoders is more attractive in applications due to low cost. Compared with the conventional PI control, the performance of MPC is better, because it can achieve faster response, bigger equivalent gain when the input is small, and vice versa. However, the conventional MPC has a defect at the zero-servo operation which is included in the process of elevator startup which is shown in Section III-A. Therefore, investigating a robust MPC method with good dynamic performance which is compatible for an ordinary resolution incremental encoder during elevator startup is definitely significant.

III. Enhanced MPC for Rollback Mitigation During the Elevator Startup

A. Analysis of the Conventional MPC

According to [27], [28], the conventional MPC is illustrated, in order to explain the drawbacks of conventional MPC during the zero-speed operation. The mechanical model of the traction machine is expressed in Laplace domain

$$\omega_f(s)=\frac{T_e(s)-T_d(s)}{Js+B} \tag{5}$$

where ω_f is the angular speed feedback generated from the raw speed, T_d represents all uncertain disturbances including the influence of the rigidity and damper of rope, B is the friction factor, and s is the Laplace operator. The disturbance T_d is usually ignored in the conventional predictive model. After zero-order-hold discretization of (5) and iteration, the discrete predictive model can be expressed as

$$\begin{aligned}\omega_m(k+n)=\ & K_m(1-\alpha_m)(1+\alpha_m+\cdots+\alpha_m^{n-1})i_q^*(k) \\ & +\alpha_m^n\omega_m(k),\ n=1,2,\ldots,P\end{aligned} \tag{6}$$

where $\omega_m(k+n)$ represents the predictive angular speed at time $k+n$, $K_m=K_{to}/J_o$, $K_{to}=1.5n_p\psi_f$; n_p is the number of pole pairs; ψ_f is the rotor flux; J_o is the nominal values of the total inertia and $\alpha_m=\exp(B_oT_s/J_o)$; B_o is the nominal values of the friction factor; T_s is the sampling period; P is the predictive step; and $i_q^*$is the reference q-axis current. Since $i_q^*\approx i_q$, i_q is replaced by i_q^* in (6). Therefore, the outputs of the predictive model at time k, $k+1, k+2\cdots k+P$ can be converted into a matrix form as follows:

$$\boldsymbol{W}_m(k)=\boldsymbol{W}_f(k)+\boldsymbol{W}_s(k)i_q^*(k) \tag{7}$$

where $W_m(k)$, $W_f(k)$, and $W_s(k)$ are expressed as

$$\begin{cases} \boldsymbol{W_m}(k)=\begin{bmatrix}\omega_m(k+1) & \cdots & \omega_m(k+P)\end{bmatrix}^T \\ \boldsymbol{W_f}(k)=\begin{bmatrix}\alpha_m & \cdots & \alpha_m^P\end{bmatrix}^T\omega_f(k) \\ \boldsymbol{W}_s(k)=K_m(1-\alpha_m)\begin{bmatrix}1 & \cdots & 1+\alpha_m\cdots+\alpha_m^{P-1}\end{bmatrix}^T. \end{cases} \tag{8}$$

In this predictive control method, to some degree, the actual speed will be closer to the trajectory speed with a larger predictive step, but it will cause huge computation amount which cannot be executed completely in a limited control period. The reference trajectory and the cost function also affect the computation amount.

The first-order exponential function is chosen as the reference trajectory which is expressed as follows:

$$\omega_r(k+n)=\omega^*(k+n)-\alpha_r^n[\omega^*(k)-\omega(k)] \tag{9}$$

where $\omega_r$is the reference trajectory and $\omega^*$is the setpoint value, which is zero during the elevator startup. $\alpha_r=e^{-T_s/T_r}$, in

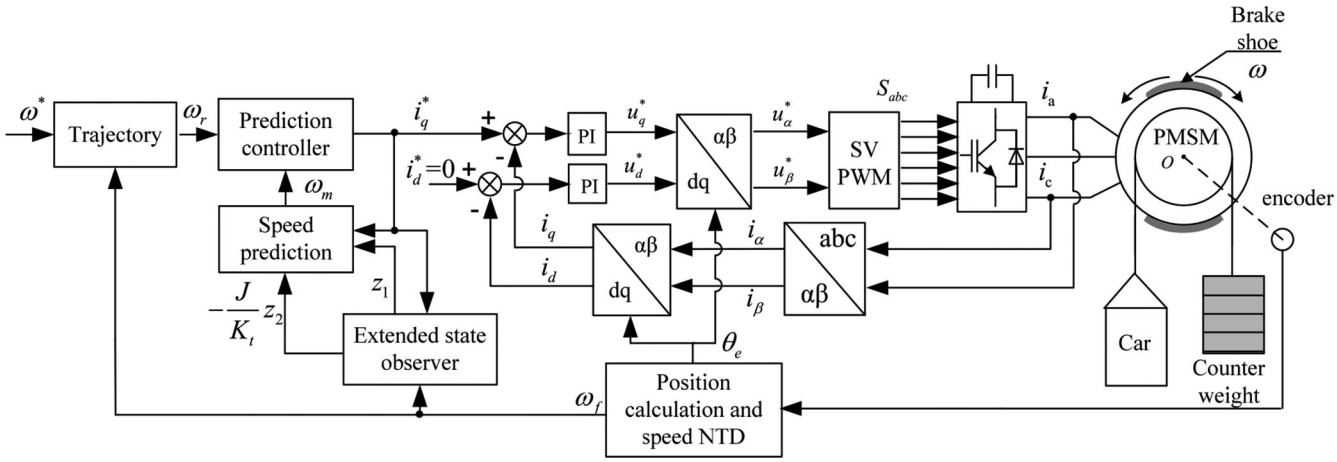

Fig. 3. Scheme of the enhanced-MPC strategy for traction machine to mitigate rollback during elevator startup.

which T_r is the time constant related to the desired response time. Considering the effect of the external disturbance and the noise, there will be an error between outputs of the predictive model and the real plant. Therefore, a corrector should be added into the predictive cost function. The predictive error *e* can be expressed as

$$e(k+P-1)=\cdots=e(k+1)=e(k)=\omega_f(k)-\omega_m(k). \tag{10}$$

The second-order cost function J_p is chosen as follows:

$$\begin{aligned} J_P=&\ [\boldsymbol{W}_r(k)-\boldsymbol{W}_m(k)-\boldsymbol{E}(k)]^{\mathrm{T}} \\ &\times\boldsymbol{Q}\,[\boldsymbol{W}_r(k)-\boldsymbol{W}_m(k)-\boldsymbol{E}(k)]+Ri_q^{*2} \end{aligned} \tag{11}$$

where $\mathbf{Q}=\mathrm{diag}\,[q_1^2 \quad \ldots \quad q_P^2]$, $R=r^2, \boldsymbol{W}_r(k)=[\omega_r(k+1)]\ldots\omega_r(k+P)^T, \boldsymbol{E}(k)=[e(k+1)\ldots e(k+P)]^T\cdot q_1, q_2 \ldots q_p$ are the weight variables for predictive steps, and *R* is the weight variable of the output current. Let $\partial J_p/\partial i_q^*=0$, the output of the MPC controller can be obtained

$$\begin{aligned} i_q^*(k)=&\ (\boldsymbol{W}_s^T\boldsymbol{Q}\boldsymbol{W}_s+R)^{-1}\boldsymbol{W}_s \\ &\boldsymbol{Q}[\boldsymbol{W}_a(\omega^*(k)-\omega_f(k))-\boldsymbol{W}_b\omega_m(k)] \end{aligned} \tag{12}$$

where $\boldsymbol{W}_a(k)=[(1-\alpha_r) \quad \ldots \quad (1-\alpha_r^P)]^{\mathrm{T}}$, $\boldsymbol{W}_b(k)=[(1-\alpha_m) \quad \ldots \quad (1-\alpha_m^P)]^{\mathrm{T}}$, and $i_q^*(k)$ is used as the *q*-axis reference current of the PI current regulator.

From (12), during the elevator startup, ω^* should be set as zero. If the conventional MPC works well, ω_f and ω_m should converge to zero. Then, the elevator car can maintain standstill during the zero-servo operation. If all the conditions analyzed above are met, $i_q^*(k)$will be zero since MPC is equivalent to a proportional controller, but if $i_q^*(k)$equals zero, the electromagnetic torque generated by $i_q^*(k)$ cannot balance the disturbance torque. The sliding speed ω_f would not be zero. Therefore, it is a self-contradiction.

Therefore, the real situation is that the sliding speed ω_f, which is a fixed value during the zero-servo operation, maintains the output of electromagnetic torque to balance the disturbance torque. The conventional MPC is not suitable to regulate the speed loop during the elevator startup.

B. Establishment of the Enhanced MPC Speed Controller for Elevator Startup

In order to overcome the drawbacks of the conventional MPC, an enhanced MPC is proposed, and the scheme is shown in Fig. 3. The enhanced MPC strategy is used instead of the conventional PI regulator in the speed loop. Additionally, the NTD is used to improve the precision of the speed feedback. The precise speed feedback information is used in trajectory and ESO blocks to generate the speed trajectory and the disturbance information, respectively, and the disturbance information is used in the speed prediction. The angular speed trajectory and predictive speeds are used as the inputs of the prediction controller. After calculation, the *q*-axis current reference is generated to control the electromagnetic torque.

MPC will cause relatively large steady-state error, if the disturbance is intense and unknown. Therefore, the ESO scheme is designed to mitigate the negative effects caused by the unknown external disturbance and reduce the sliding distance. The receding optimization can enhance the robustness against load disturbance during the elevator startup process.

In order to consider and analyze the influence of coefficient mismatch and disturbance, (5) can be changed into

$$\dot{\omega}_f(t)=\frac{K_{to}+K_{t\Delta}}{J_o+J_\Delta}i_q^*(t)-\frac{B_o+B_\Delta}{J_o+J_\Delta}\omega_f(t)-\frac{T_d(t)}{J_o+J_\Delta} \tag{13}$$

where $K_{t\Delta}$ is the mismatch error of K_{to}, J_Δ and $B_\Delta$are the mismatch errors of the total inertia and the friction factor, and J_o and $B_o$are the nominal values of the inertia and the friction factor, respectively. In order to obtain the predictive state equation, (13) can be expressed as follows:

$$\begin{cases} \dot{\omega}_f(t)=\dfrac{K_{\mathrm{to}}}{J_o}i_q^*(t)-\dfrac{B_o}{J_o}\omega_f(t)-\dfrac{K_{\mathrm{to}}}{J_o}i_{qd}(t) \\ i_{qd}(t)=-\dfrac{T_d(t)}{K_{\mathrm{to}}}+\dfrac{K_{t\Delta}}{K_{\mathrm{to}}}i_q^*(t)-\dfrac{B_\Delta}{K_{\mathrm{to}}}\omega_f(t)-\dfrac{J_\Delta}{K_{\mathrm{to}}}\dot{\omega}_f(t) \end{cases} \tag{14}$$

where i_{qd} includes the equivalent current of uncertain disturbance torque T_d and the mismatch error of both the inertia and the friction factor. The estimated value of i_{qd} can be generated

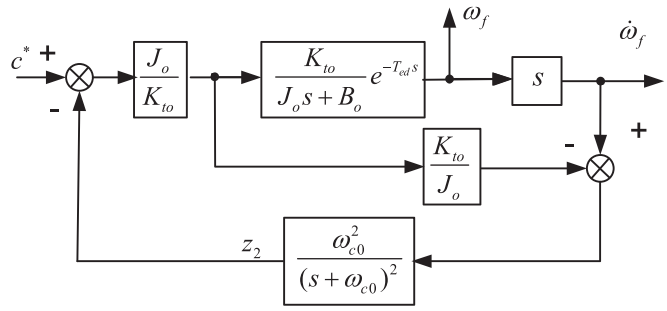

Fig. 4. Equivalent structure of the ESO.

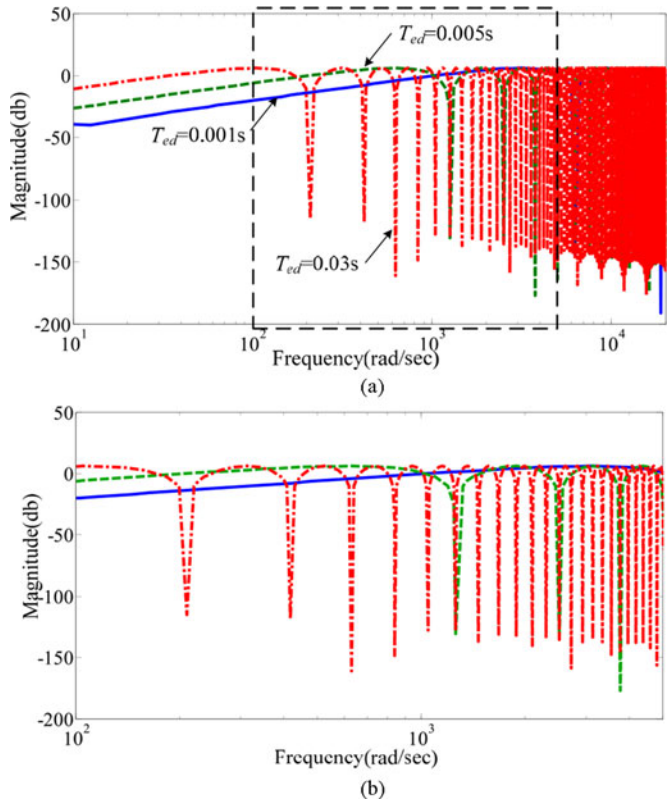

Fig. 5. Influence of the equivalent filter parameters on $M(\omega)$. (a) Bode diagram. (b) Magnified Bode diagram.

by ESO, so the mismatch of the predictive model can be compensated. During the elevator startup, the uncertain disturbance torque exerting on the traction sheave can be traced accurately and quickly. After zero-order-hold discretization of (14) and iteration, it can be expressed as

$$\omega_m(k+n) = K_m(1-\alpha_m)(1+\alpha_m+\cdots+\alpha_m^{n-1}) [i_q^*(k) - i_{qd}(k)] + \alpha_m^n \omega_m(k),\ n=1,2,\ldots,P. \tag{15}$$

In (15), the disturbance has been considered in the predictive model, which is different from (6). The uncertain disturbance torque can be treated as a constant because of short-sampling period. Therefore, the estimated disturbance and speed generated from ESO can be utilized to adjust the predictive model during each sampling period; thus, enhancing robustness against the uncertain disturbance torque.

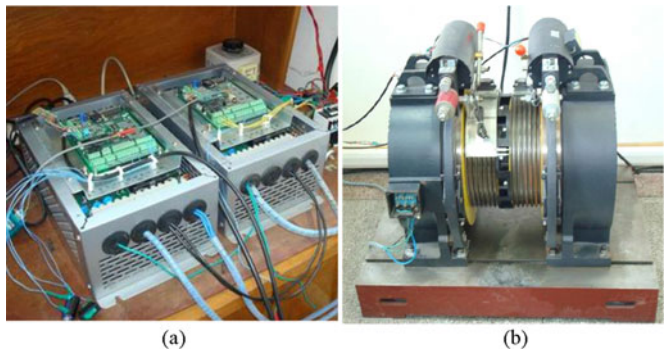

Fig. 6. Experimental platform of 11.7-kW direct-drive permanent magnet traction machines. (a) Traction machine drivers. (b) Load test platform.

The disturbance affecting the output can be extended into a new state by using an ESO. In other words, the ESO is established to obtain this new state by a special feedback structure. It does not depend on the specific mathematical model to obtain the disturbance information, and does not need to measure its effect directly. According to these characteristics, it is suitable and practical to use ESO to estimate the equivalent load torque of the traction machine during the elevator converts from a standby mode to the running mode.

According to (14), the ESO can be established as follows:

$$\begin{cases} \dot{z}_1(t) = z_2(t) + \alpha_{01}(\omega_f(t) - z_1(t)) + \dfrac{K_{\rm to}}{J_o} i_q^*(t) - \dfrac{B_o}{J_o}\omega_f(t) \\ \dot{z}_2(t) = \alpha_{02}(\omega_f(t) - z_1(t)) \end{cases} \tag{16}$$

where z_1 and z_2 are two variables of the ESO, α_{01} and α_{02} are parameters of the ESO, $z_1(t) \to \omega_f(t)$ and $z_2(t) \to -K_{\rm to} i_{qd}(t)/J_o$. Therefore, the equivalent current component of disturbance torque i_{qd} and the initial predictive speed can be obtained. After discretization of (16), it can be expressed as

$$\begin{cases} z_1(k+1) = (1 - T_s\alpha_{01}) z_1(k) + T_s(z_2(k) \\ \qquad\qquad + \left(\alpha_{01} - \frac{B_o}{J_o}\right)\omega_f(k) + \frac{K_{\rm to}}{J_o} i_q^*(k)) \\ z_2(k+1) = z_2(k) + T_s\alpha_{02}(\omega_f(k) - z_1(k)). \end{cases} \tag{17}$$

Then in (15), $\omega_m(k)$ and $i_{qd}(k)$ are replaced by $z_1(k)$ and $-J_o z_2(k)/K_{\rm to}$, respectively. The initial value of predictive speeds within the predictive step P can be rolling corrected during each sampling period, so (18) can be obtained as

$$\omega_m(k+n) = K_m(1-\alpha_m)(1+\alpha_m+\cdots+\alpha_m^{n-1}) \times \left[i_q^*(k) + \frac{J_o}{K_{\rm to}} z_2(k)\right] + \alpha_m^n z_1(k), \quad n=1,2,\ldots,P. \tag{18}$$

Therefore, the outputs of the predictive model at time k, $k+1, k+2 \cdots k+P$ can be converted into a matrix form as follows:

$$\boldsymbol{W}_m(k) = \boldsymbol{W}_f(k) + \boldsymbol{W}_s(k)\left[i_q^*(k) + \frac{J_o}{K_{\rm to}} z_2(k)\right]. \tag{19}$$

In the ESO, the initial predictive speed has been corrected at each sampling time. Therefore, the function of correcting the initial predictive speed can be eliminated, which can effectively reduce the computational burden. Moreover, the predictive error caused by the disturbance has been corrected in the predictive model. There is no need correcting it in the cost function anymore like (11). If the third order or above is used in the cost function, the computational process would be too complicated, and the processor may not complete the computation in the fixed time, but the first order cannot meet the requirement of fast response. The second-order cost function of the enhanced MPC is chosen as follows:

$$J_P = [\boldsymbol{W}_r(k) - \boldsymbol{W}_m(k)]^{\mathrm{T}} \boldsymbol{Q} [\boldsymbol{W}_r(k) - \boldsymbol{W}_m(k)] + R i_q^{*2}. \tag{20}$$

Let $\partial J_p / \partial i_q^* = 0$, the output of the enhanced model predictive controller can be obtained as

$$i_q^*(k) = (\boldsymbol{W}_s^{\mathrm{T}} \boldsymbol{Q} W_s + R)^{-1} \boldsymbol{W}_s^{\mathrm{T}} \boldsymbol{Q} \left[\boldsymbol{W}_r(k) - \boldsymbol{W}_f(k) + \boldsymbol{W}_s \frac{J_o}{K_{\mathrm{to}}} z_2(k) \right]. \tag{21}$$

Additionally, there should be some variable constraints in the enhanced controller. Let I_{qo} represents the rated value of i_q. Therefore, $-I_{qo} \le i_q^* \le I_{qo}$ should be met. In order to avoid the intense vibration, $-15\% I_{qo} \le i_q^*(k) - i_q^*(k-1) \le 15\% I_{qo}$ should be met, and to improve the robustness, ω_m should be restricted to a scale from $-10\%\omega_{mo}$ to $10\%\omega_{mo}$ where ω_{mo} is the nominal value of the mechanical angular velocity.

C. Stability Analysis and Parameter Selection of the ESO

In this part, the stability of the proposed method is analyzed first, because many variables are involved and the design is relatively complicated. To begin with, let $I_{qd}(t) = -K_{\mathrm{to}} i_{qd}(t)/J_o$ to simplify the arithmetic and show the process clearly. Because the sliding speed ω_f and B are relatively small, $B_o \omega_f(t)/J_o$ can be ignored when analyzing the stability. Then, (14) can be rearranged into the state form

$$\begin{bmatrix} \dot{\omega}_f(t) \\ \dot{i}_{qd}(t) \end{bmatrix} = \begin{bmatrix} 0 & 1 \\ 0 & 0 \end{bmatrix} \begin{bmatrix} \omega_f(t) \\ i_{qd}(t) \end{bmatrix} + \begin{bmatrix} \frac{K_{\mathrm{to}}}{J_o} i_q^*(t) \\ c(t) \end{bmatrix} \tag{22}$$

where $c(t)$ is the rate of change of $i_{qd}(t)$, and (9) can be written as the state form

$$\begin{bmatrix} \dot{z}_1(t) \\ \dot{z}_2(t) \end{bmatrix} = \begin{bmatrix} -\alpha_{01} & 1 \\ -\alpha_{02} & 0 \end{bmatrix} \begin{bmatrix} z_1(t) \\ z_2(t) \end{bmatrix} \begin{bmatrix} \alpha_{01} & 1 \\ \alpha_{02} & 0 \end{bmatrix} \begin{bmatrix} \omega_f(t) \\ 0 \end{bmatrix} + \begin{bmatrix} \frac{K_{\mathrm{to}}}{J_o} i_q^*(t) \\ c(t) \end{bmatrix} \tag{23}$$

By subtracting (22) from (23), the error equation can be obtained

$$\begin{bmatrix} \dot{z}_1(t) - \dot{\omega}_f(t) \\ \dot{z}_2(t) - \dot{i}_{qd}(t) \end{bmatrix} = \begin{bmatrix} -\alpha_{01} & 1 \\ -\alpha_{02} & 0 \end{bmatrix} \begin{bmatrix} z_1(t) - \omega_f(t) \\ z_2(t) - i_{qd}(t) \end{bmatrix} \tag{24}$$

$$\text{Let} \begin{cases} e_1(k) = z_1(k) - \omega_f(k) \\ e_2(k) = z_2(k) - i_{qd}(k) \end{cases}, e = \begin{bmatrix} e_1(t) \\ e_2(t) \end{bmatrix}, \text{then}$$

$$\dot{e} = \begin{bmatrix} -\alpha_{01} & 1 \\ -\alpha_{02} & 0 \end{bmatrix} e. \tag{25}$$

According to Routh–Hurwitz criterion, if $\alpha_{01} > 0$and $\alpha_{02} > 0$, the ESO is stable. So if these parameters are chosen suitably, the system can be stable and makes $z_1 \to \omega_f$ and $z_2 \to i_{qd}$ fast.

In order to facilitate the analysis, the ESO parameters are selected as$\alpha_{01} = 2\omega_{c0}$, $\alpha_{02} = \omega_{c0}^2$, in which ω_{c0} is the bandwidth of the ESO. According to (16), the structure of the ESO can be described as an internal model control structure, which is shown in Fig. 4. The model of ESO is equivalent to the differential of the real plant. Therefore, the transfer function of the plant model is obtained

$$G_p(s) = \frac{K_{to} s}{J_o s + B_o} e^{-T_{\mathrm{ed}} s} \tag{26}$$

where T_{ed} is the equivalent delay time mainly caused by speed sampling, low-pass filter, and digital control delay. The relevant part of the model can be expressed as

$$G_m(s) = \frac{K_{to}}{J_o}. \tag{27}$$

The transfer functions of the controller and the extended state conversion can be, respectively, described as

$$G_{\mathrm{imc}}(s) = \frac{J_o}{K_{to}} \tag{28}$$

$$F_{\mathrm{imc}}(s) = \frac{\omega_{c0}^2}{(s + \omega_{c0})^2}. \tag{29}$$

From (26)–(29), the multiplicative uncertainty expression and the complementary sensitivity function are shown as follows:

$$M(s) = \frac{G_p}{G_m} - 1 = \frac{J_o s}{J_o s + B_o} e^{-T_{ed} s} - 1 \tag{30}$$

$$\delta(s) \approx G_m \cdot G_{\mathrm{imc}} \cdot F_{\mathrm{imc}} = \frac{\omega_{c0}^2}{(s + \omega_{c0})^2}. \tag{31}$$

To guarantee the robustness of the internal model control, the condition should be met

$$\|\delta(\omega) M(\omega)\|_\infty = \sup_\omega |\delta(\omega) M(\omega)| < 1. \tag{32}$$

Substitute (30) and (31) into (32), then the result can be obtained

$$\sup_\omega |\delta(s) M(s)| = \sup_\omega \left| \frac{\omega_{c0}^2}{(j\omega + \omega_{c0})^2} \left[\frac{J_o j\omega}{J_o j\omega + B_o} e^{-T_{ed} j\omega} - 1 \right] \right| < 1. \tag{33}$$

According to (31), as ω_{c0} increases, the bandwidth of $\delta(\omega)$ extends to high frequency. The possibility that $\sup_\omega |\delta(\omega) M(\omega)|$ becomes greater than 1 will increase, which means the stability of the system deteriorates. The equivalent delay time T_{ed} of the observer can be expressed in Bode diagram graphically.

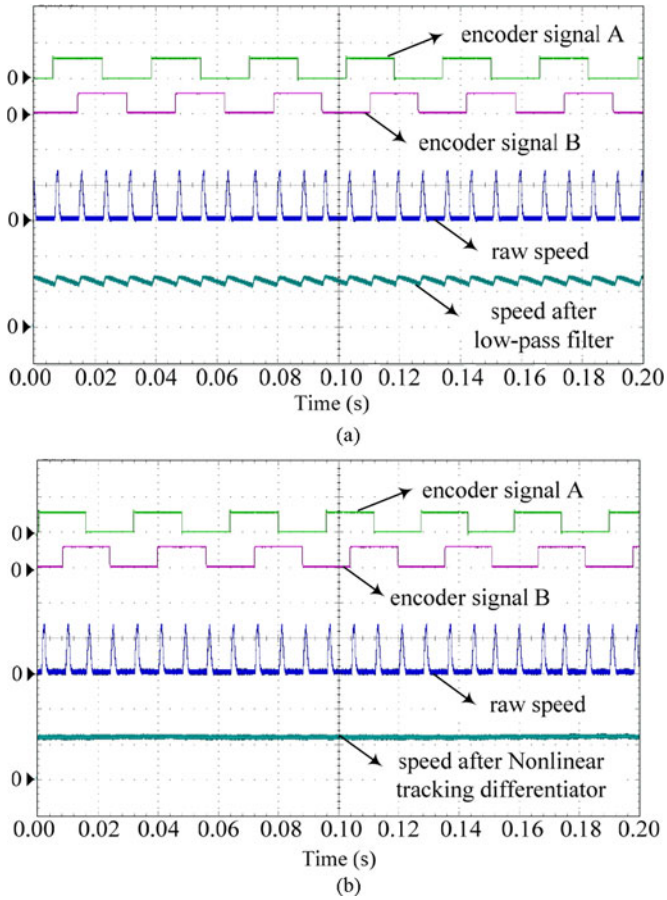

Fig. 7. Comparison of the experimental waveforms of sampling speeds using low-pass filter and NTD. (a) Using the low-pass filter. (b) Using the NTD.

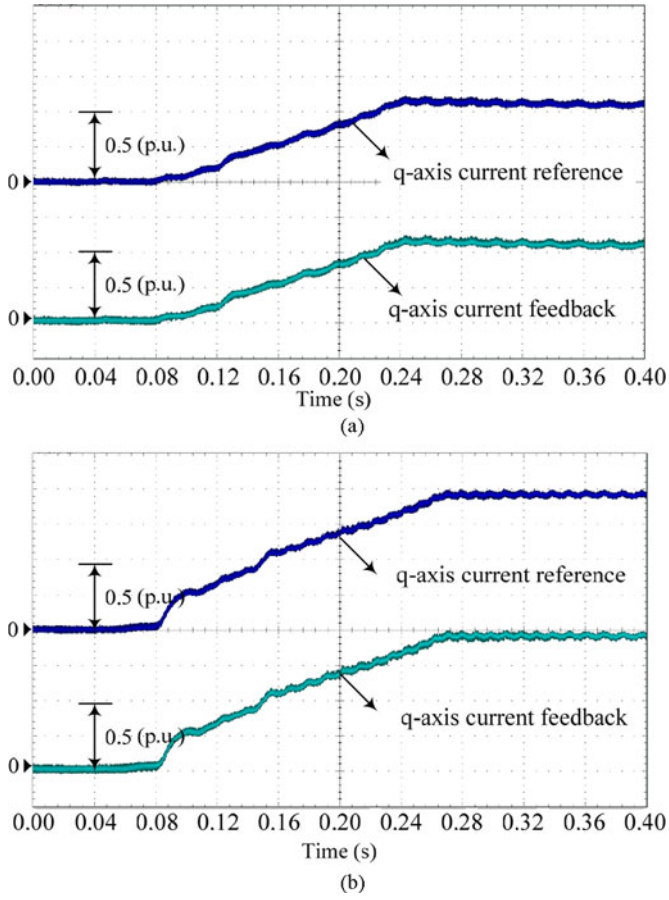

Fig. 8. Experimental comparison of q-axis reference and feedback currents under different loads. (a) Under 60% rated load. (b) Under rated load.

When $T_{\rm ed}$ is equal to 0.001, 0.005, and 0.03, respectively, the Bode diagram of $M(\omega)$ is shown in Fig. 5. As $T_{\rm ed}$ increases, the frequency of peak amplitude of $M(\omega)$ reduces. Therefore, the possibility of $\sup_\omega |\delta(\omega)M(\omega)|$ becoming greater than 1 will increase, which means the stability of the system will also deteriorate.

It is necessary to take the performance requirements, the stability of ESO and the quick adjustment, together into consideration when choosing ω_{c0} and T_{ed}. Therefore, when selecting ω_{c0}, both the convergence speed and the stability of the ESO should be considered. If ω_{c0} is relatively large, the convergence speed of ESO increases, but the stability of the system will be impaired. Therefore, based on the requirements of the real plant, the parameter ω_{c0} needs to be carefully adjusted. Additionally, $T_{\rm ed}$ is mainly decided by the speed sampling method and raw speed processing method. Usually, the sampling period is fixed, so it is important to adopt a suitable raw speed processing method.

D. Application of the NTD in Speed Sampling

Based on the analysis above, the equivalent delay time $T_{\rm ed}$ significantly affects the stability of the ESO. Therefore, T method and M/T method are difficult to be used in speed detection because of the variable speed sampling time. Additionally, the sliding speed during the elevator startup is relatively small when the starting torque control algorithm performs effectively. Conventionally, the raw speed signal is obtained by using M method. Then, the speed feedback can be got after processing the raw speed through a low-pass filter. However, the speed feedback not only contains noise and vibration, but also have a large time delay caused by the filter. Under the circumstances of rollback mitigation requiring accurate adjustment, these disadvantages will obviously deteriorate the control performance and cause mechanical vibration at steady state.

NTD was originally proposed by Han [29]. It can be used to extract continuous signals and differential signals from noncontinuous signals. When the parameters are selected carefully, it has a shorter time delay and stronger noise suppression ability than the conventional low-pass filter. Therefore, this method can be used to process the raw speed signal as a high-performance filter.

The state equation of NTD can be expressed as follows:

$$\begin{cases} \omega_f(k+1) = \omega_f(k) + T_s\omega_d(k) \\ \omega_d(k+1) = \omega_d(k) + T_s nlf(\omega_f(k) - \omega(k), \omega_d(k), R, H_0) \end{cases} \tag{34}$$

where R is the convergence factor, H_o is the filtering factor, mainly affecting the filtering effect, ω_d is the rate of change of ω_f, ω is the raw speed, and the nonlinear function $nlf(\omega_f(k) - \omega(k), \omega_d(k), R, H_0)$ can be defined as follows:

$$nlf(\omega_f(k) - \omega(k), \omega_d(k), R, H_0)$$

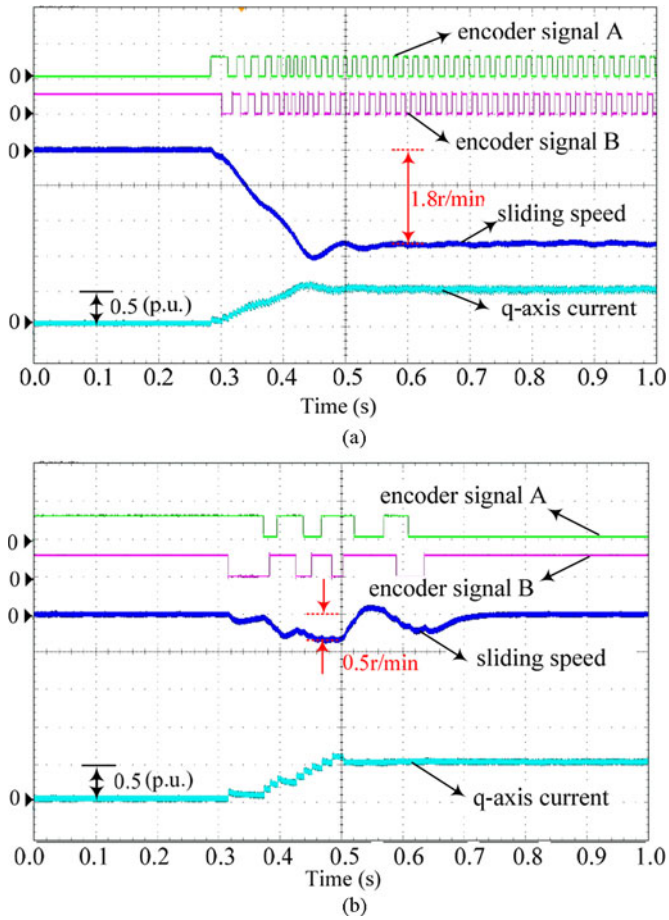

Fig. 9. Experimental comparison of the two methods under 60% rated load. (a)Conventional MPC without the ESO. (b) Enhanced MPC with the ESO.

$$= -\begin{cases} R\text{sign}(A), & |A| > D \\ R\frac{A}{D}, & |A| \le D \end{cases} \tag{35}$$

where

$$A = -\begin{cases} \omega_d(k) + \dfrac{A_0 - D}{2}\text{sign}(y), & |y| > D_0 \\ \omega_d(k) + \dfrac{y}{H_0}, & |y| \le D_0 \end{cases} \tag{36}$$

$$A_0 = \sqrt{D^2 + 8R|y|} \tag{37}$$

$$y = \omega_f(k) - \omega(k) + H_0\omega_d(k) \tag{38}$$

$$D_0 = H_0 D \tag{39}$$

$$D = RH_0. \tag{40}$$

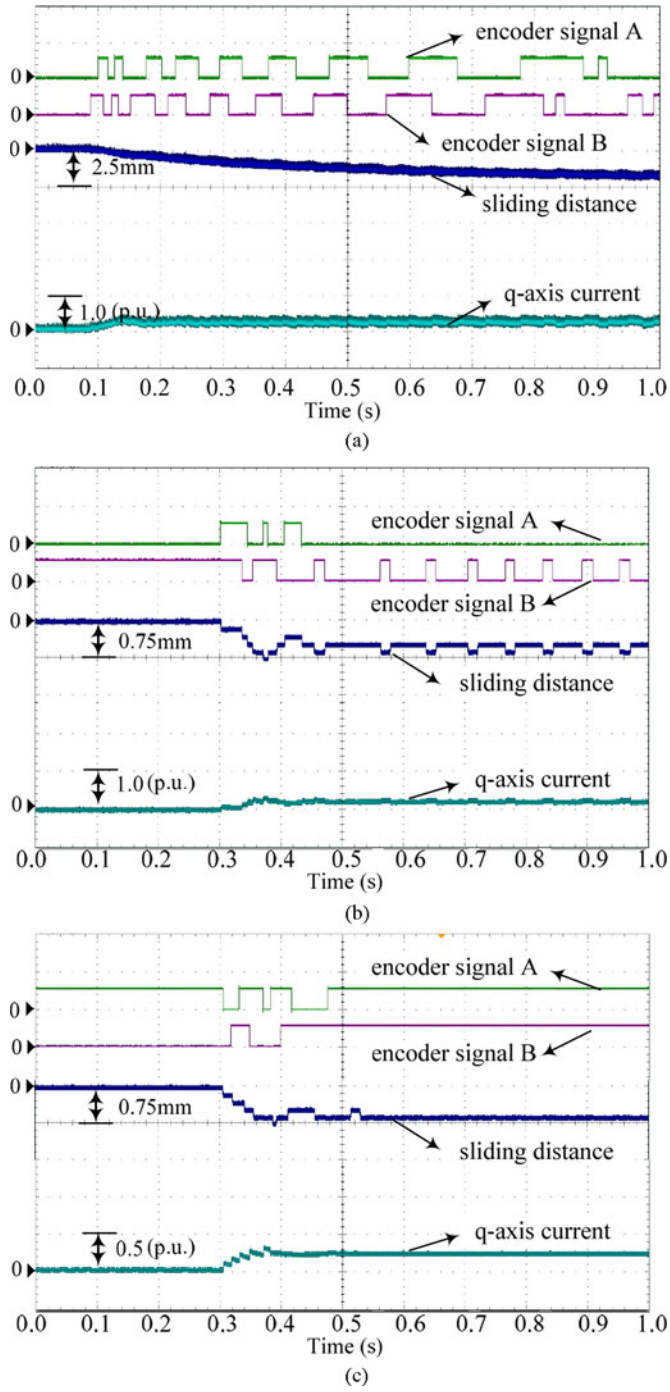

Fig. 10. Experimental comparison of the three methods under 20% rated load. (a) PI speed regulator. (b) Enhanced MPC with low-pass filter. (c) Enhanced MPC with NTD.

E. Analysis of Parameter Selection

1) Parameters of MPC: The larger the predictive step P is, the longer the executive time of the control algorithm would become. Considering a fixed-point DSP-based commercial drive is used in the experiment, the predictive step is selected as 5, which can both ensure the predictive accuracy and reduce the computational burden. In terms of weight factor of each predictive step, it can be selected as large as possible on the premise that overshoot and strong vibrations should be avoided, and the weight factor reflects the importance of each step. Normally, the weight factor of the former step is larger than that of the latter one, because the former one is more precise than the latter one with the same i_q^* at the time k. The weight factor of i_q^* should be a little smaller considering the dynamics of the control strategy. If the weight factor of i_q^* is relatively large, the change of i_q^* at each sampling time would be restricted to a small scale. The trajectory coefficients are selected according to how fast the actual speed approaching to the trajectory is expected.

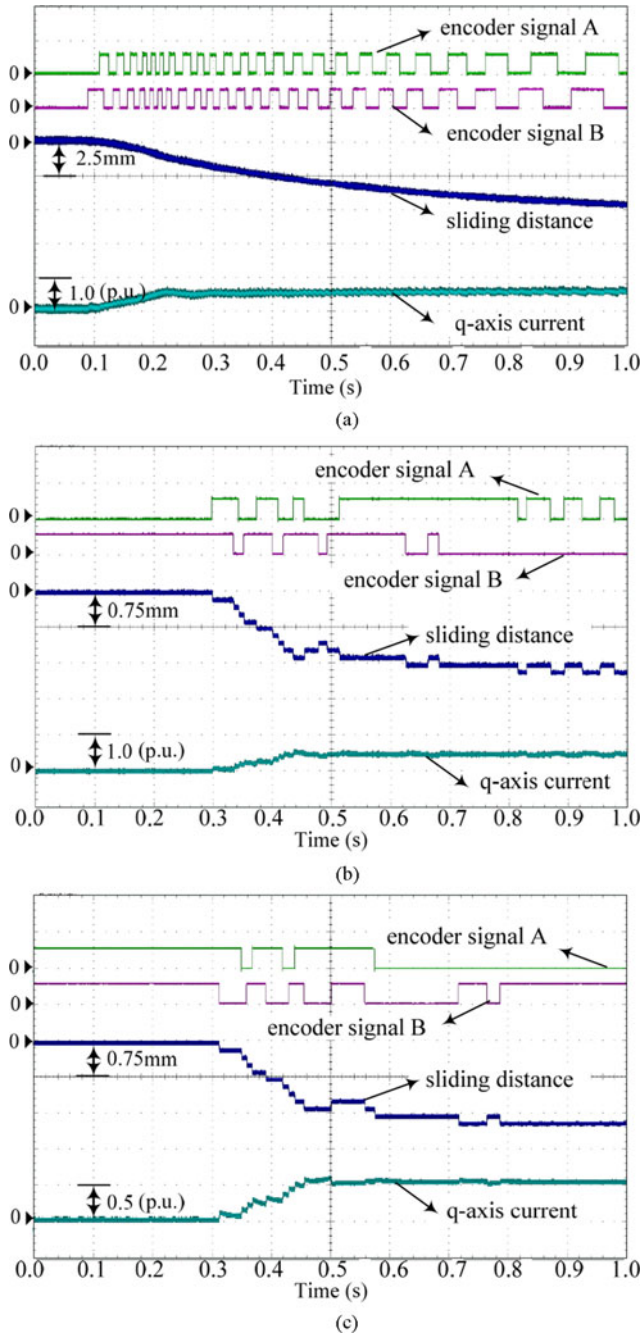

Fig. 11. Experimental comparison of the three methods under 60% rated load. (a) PI speed regulator. (b) Enhanced MPC with low-pass filter. (c) Enhanced MPC with NTD.

2) Parameters of ESO: According to the second-order system expression (29), the settling time t_s and the overshoot are the main dynamic performance factors, and the overshoot needs to be zero because of the requirement of the antirollback control. Therefore, only t_s is taken into account when choosing ω_{c0}. So using a unit step disturbance as the input, and the response of (29) can be expressed as

$$F_{\mathrm{imc}}(t) = 1 - \omega_{c0} t e^{-\omega_{c0} t} = 1 - (1 + \omega_{c0} t) e^{-\omega_{c0} t}. \quad (41)$$

According to the definition of the settling time, $|F_{\mathrm{imc}}(t_s) - F_{\mathrm{imc}}(\infty)| = \lambda$, where $F_{\mathrm{imc}}(\infty) = 1$ and $\lambda \triangleq 2\%$, then the result can be got as

$$(1 + \omega_{c0} t_s) e^{-\omega_{c0} t_s} = 0.02. \quad (42)$$

After calculation, the relation between t_s and ω_{c0} can be obtained

$$t_s = 5.85/\omega_{c0}. \quad (43)$$

However, considering there are some differences between the real system and the ideal one, design margins should be reserved to make the system be robust. So the equation below can be used to decide ω_{c0}

$$t_s = 15/\omega_{c0}. \quad (44)$$

3) Parameters of NTD: Since *R* is the convergence factor, it determines the tracking performance of the rotor speed. The larger *R* is, the better tracking ability is, but the high-frequency noise will be caused, if *R* is relatively large. According to [26], the scale of *R* can be selected from 500 to 1000 with no high-frequency noise existing. If the noise is contained in the output, the filtering factor H_o should be adjusted to reduce the influence of noise. On the premise that the tracking performance can be ensured, *R* should be selected as small as possible. Usually, the range of H_o can be from 0.00002*R* to 0.00004*R*, which guarantees both the filter performance and time lag limitation.

IV. Experimental Validation

A. Experimental Setup

The proposed rollback mitigation control strategy was verified on an 11.7-kW elevator traction machine using a commercial inverter, and the experimental platform is shown in Fig. 6, a same type traction machine is mechanically connected to emulate the load of elevator car. Parameters of the permanent magnet traction machine used in the experiment are shown in Table A1. The PWM frequency of inverter is 10 kHz. The whole control algorithm is executed by a TMS320F2808 DSP chip. The control period of speed loop is 1 ms.

According to the analysis in Section III, the parameters of enhanced MPC are selected in experiments as follows: $P = 5$, $\alpha_m = 0.98$, $q_1 = 15$, $q_2 = 11$, $q_3 = 8$, $q_4 = 5$, $r = 0.1$, and $T_s = 1$ ms. The parameter ω_{c0} of ESO is set as 250. The NTD parameters are selected as follows: $R = 500$ and $H_0 = 0.015$.

In order to compare the proposed method with the conventional PI cascade control system, parameters of the speed PI controller ($k_p = 35$, $k_i = 100$) have been regulated to the optimum, which means they cause acceptable vibration at steady state and can make the response of speed loop and current loop as fast as possible to reduce the sliding distance. An encoder with an ordinary resolution of 2048 was installed on the machine, and only the orthogonal pulse signals A and B were used for the rollback mitigation control.

B. Performance of NTD

The performance of tracking and filtering can be changed with different parameters of NTD. The NTD parameters are selected as follows: $R = 500$ and $H_0 = 0.015$, and the cut-off frequency of the low-pass filter is 17 Hz. When the speed of

the traction machine is 2 r/min, the experimental waveforms of sampling speeds using the low-pass filter and the NTD are shown, respectively, in Fig. 7(a) and (b). The middle waveform is the raw speed signal, and the bottom waveforms in Fig. 7(a) and (b) are the speed signal through the low-pass filter and the NTD, respectively. From the results, the speed signal obtained by using NTD is smoother, with less vibration at low-speed region.

C. Performance of the Internal Current Loop Adopting PI Regulator

The whole control strategy is ultimately executed by a fixed-point DSP chip, in which the current loop regulating period is one-tenth of the speed loop. The response of the current loop using an optimal PI controller is sufficiently fast for this direct-drive application from experimental results as shown in Fig. 8. So if the parameters of PI controller are well designed, it can make the current feedback trace the current reference well for achieving effective rollback mitigation. The most important thing in resolving the rollback problem is that the output of the speed controller must match the uncertain and changing load torque. Compared with the MPC regulating both internal and external loops, the enhanced MPC strategy can not only increase the robustness of the system, but also effectively reduce the amount of calculation.

D. Experimental Comparison Between Conventional and Proposed Enhanced MPC

An experimental comparison between conventional MPC without ESO and enhanced MPC with ESO under 60% rated load was carried out. The experimental results are shown in Fig. 9. The middle waveform is the sliding speed, and the bottom waveform is the q-axis current. From Fig. 9, the traction sheave is still sliding at the speed of 1.8 r/min when using the conventional MPC, the reason is that the q-axis current used to balance the disturbance is generated by the steady-state speed error which should be prevented. The steady-state speed error will cause the elevator car sliding.

E. Control Performance Comparison of PI, Conventional MPC, and Proposed Enhanced MPC

Under the same experimental conditions, the experimental results of the PI speed regulator and the enhanced MPC with NTD and with low-pass filter are compared. There is no difference in basic parameters between enhanced MPC with NTD and with low-pass filter. Figs. 10–12 show the experimental results under 20%, 60%, and 100% of rated load, respectively. In terms of the sliding distance, there is no obvious difference between the enhanced MPC with NTD and with low-pass filter. Under 20% of rated load, the sliding distance with PI speed regulator is 2.30 mm, while the sliding distance with enhanced MPC is only 0.75 mm. During the steady state, there still exists vibration when using the enhanced MPC with low-pass filter as shown in Figs. 10(b), 11(b), and 12(b). However, the vibration is eliminated when using the enhanced MPC with NTD as shown in Figs. 10(c), 11(c), and 12(c).

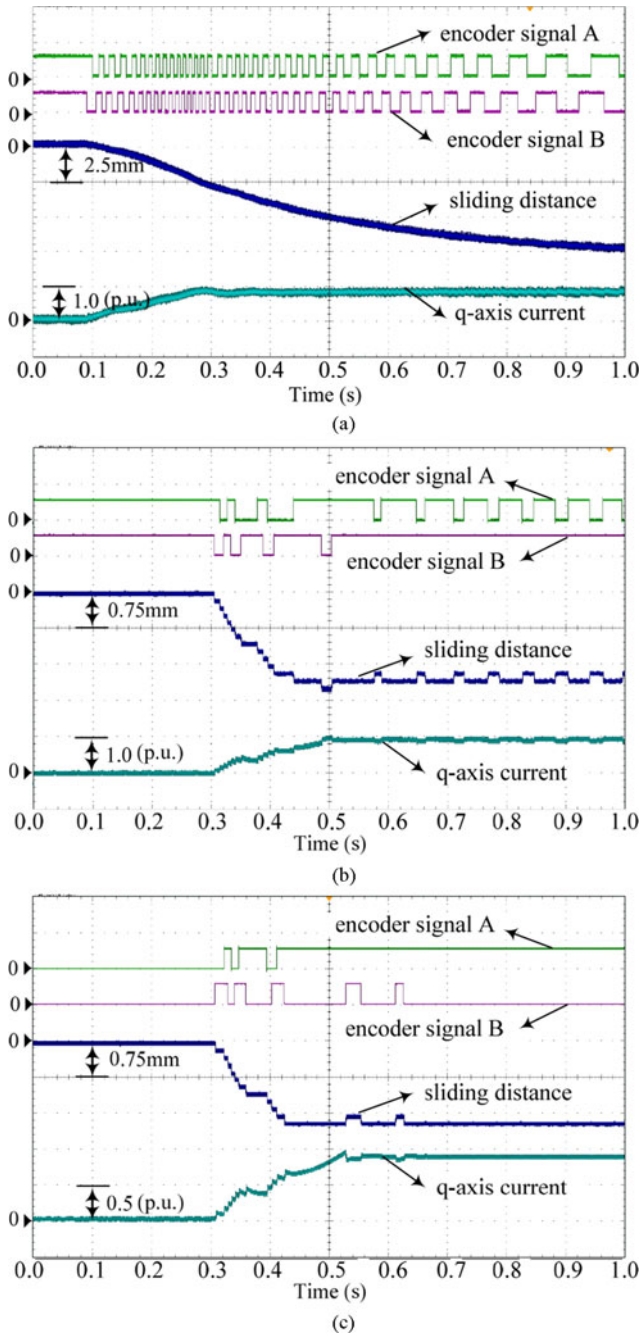

Fig. 12. Experimental comparison of the three methods under 100% rated load. (a) PI speed regulator. (b) Enhanced MPC with low-pass filter. (c) Enhanced MPC with NTD.

Under 60% of rated load, the sliding distance with PI speed regulator is 4.13 mm, while the sliding distance of enhanced MPC with NTD is only 1.50 mm. Under rated load, the sliding distance with PI speed regulator is 7.00 mm, while the sliding distance of enhanced MPC with NTD is only 1.80 mm. In summary, the proposed enhanced MPC with NTD can get much shorter sliding distance, smaller sliding speed, better riding comfort, and no vibration at steady state.

Fig. 13 shows the comparison between the PI speed regulator and the proposed enhanced MPC with NTD under different loads. From Fig. 13, the sliding distances of the proposed method are much shorter than those of PI speed regulator under

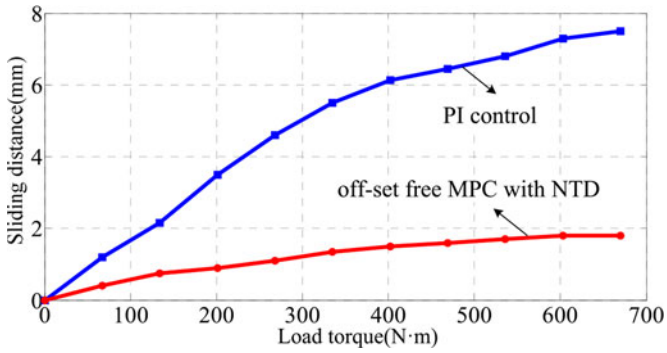

Fig. 13. Sliding distance comparison of the two methods under different loads.

different loads. Therefore, the proposed method can effectively solve the technical difficulties of weight-transducerless elevator drives.

V. Conclusion

This paper proposed a novel weight-tranducerless starting torque control strategy based on enhanced MPC with ESO for a direct-drive elevator traction system which can achieve high performance with an ordinary resolution encoder. In order to overcome the mismatch of the predictive model caused by the braking torque and the unknown car load, the ESO is used to rectify the predictive model. Both the stability and the parameter selection of the observer are analyzed. The NTD can make the speed feedback contain less vibration than the conventional low-pass filter. The estimated speed obtained from the ESO used as the initial value of the predictive speed can reduce the computational burden of the cost function. Instead of taking the conventional PI as the speed regulator, the enhanced MPC with ESO can effectively improve the dynamic performance without weight transducers, which benefits the robustness of the system. Therefore, the riding comfort can be improved when the elevator operates from the standby mode to the running mode. Experimental results verify that the proposed control strategy can achieve shorter sliding distance and smaller sliding speed without steady-state error for the direct-drive elevators installed with an ordinary resolution encoder.

Appendix A

TABLE A1
Traction Machine Parameters

Parameters	value
Rated power	11.7 kW
Rated voltage	380 V
Rated current	23 A
Rated speed	167 r/min
Rated torque	670 N · m
Stator resistance	0.23 Ω
d-axis/*q*-axis inductance	15 mH
Number of pole pairs	12
Inertia of traction machine	4.02 kg · m^2

References

[1] N. Mutoh, N. Ohnuma, A. Omiya, and M. Konya, "A motor driving controller suitable for elevators," *IEEE Trans. Power Electron.*, vol. 13, no. 6, pp. 1123–1134, Nov. 1998.
[2] J. He, C. Mao, J. Lu, and J. Yang, "Design and implementation of an energy feedback digital device used in elevator," *IEEE Trans. Ind. Electron.*, vol. 58, no. 10, pp. 4636–4642, Oct. 2012.
[3] E. Jung, H. Yoo, S. K. Sul, H. S. Choi, and Y. Y. Choi, "A nine-phase permanent-magnet motor drive system for an ultrahigh-speed elevator," *IEEE Trans. Ind. Appl.*, vol. 48, no. 3, pp. 987–995, May/Jun. 2012.
[4] I. Stamenkovic, N. Milivojevic, N. Schofield, M. Krishnamurthy, and A. Emadi, "Design, analysis, and optimization of ironless stator permanent magnet machines," *IEEE Trans. Power Electron.*, vol. 28, no. 5, pp. 2527–2538, May 2013.
[5] H. Yetis, H. Boztepeli, Y. Yasa, and E. Mese, "Comparative design of direct drive PM synchronous motors in gearless elevator systems," in *Proc. IEEE 3rd Int. Conf. Electr. Power Energy Convers. Syst.*, 2013, pp. 1–5.
[6] R. Ficheux, F. Caricchi, F. Crescimbini, and O. Honorati, "Axial-flux permanent-magnet motor for direct-drive elevator systems without machine room," *IEEE Trans. Ind. Appl.*, vol. 37 no. 6, pp. 1693–1701, Nov./Dec. 2001.
[7] J. W. Jung, V. Q. Leu, T. D. Do, E. K. Kim, and H. H. Choi, "Adaptive PID speed control design for permanent magnet synchronous motor drives," *IEEE Trans. Power Electron.*, vol. 30, no. 2, pp. 900–908, Feb. 2015.
[8] L. Niu, D. Xu, M. Yang, X. Gui, and Z. Liu, "On-line inertia identification algorithm for PI parameters optimization in speed loop," *IEEE Trans. Power Electron.*, vol. 30, no. 2, pp. 849–858, Feb. 2015.
[9] X. Zhang, L. Sun, K. Zhao, and L. Sun, "Nonlinear speed control for PMSM system using sliding-mode control and disturbance compensation techniques," *IEEE Trans. Power Electron.*, vol. 28, no. 3, pp. 1358–1365, Mar. 2013.
[10] J. Solsona and M. Valla, "Disturbance and nonlinear Luenberger observers for estimating mechanical variables in permanent magnet synchronous motors under mechanical parameters uncertainties," *IEEE Trans. Ind. Electron.*, vol. 50, no. 4, pp. 717–725, Aug. 2003.
[11] D. Grignion, X. Chen, N. Kar, and H. Qian, "Estimation of load disturbance torque for DC motor drive systems under robustness and sensitivity consideration," *IEEE Trans. Ind. Electron.*, vol. 61, no. 2, pp. 930–942, Feb. 2014.
[12] S. Bolognani, A. Faggion, L. Sgarbossa, and L. Peretti, "Modelling and design of a direct-drive lift control with rope elasticity and estimation of starting torque," in *Proc. IEEE 33rd Annu. Conf. Ind. Electron. Soc.*, 2007, pp. 828–832.
[13] X. Hong, Z. Deng, S. Wang, L. Huang, W. Li, and Z. Lu, "A novel elevator load torque identification method based on friction model," in *Proc. IEEE 25th Annu. Appl. Power Electron. Conf. Expo.*, 2010, pp. 2021–2024.
[14] G. Wang, G. Zhang, R. Yang, and D. Xu, "Robust low-cost control scheme of direct-drive gearless traction machine for elevators without a weight transducer," *IEEE Trans. Ind. Appl.*, vol. 48, no. 3, pp. 996–1005, May/Jun. 2012.
[15] F. Liu, A. Shen, Y. Zhang, and W. Fu, "A rapid and high-accuracy control scheme of starting torque for elevators without a weight transducer," in *Proc. IEEE 23rd Int. Symp. Ind. Electron.*, 2014, pp. 733–738.
[16] G. Wang, J. Xu, T. Li, G. Zhang, H. Zhan, L. Ding, and D. Xu, "Weight-transducerless starting torque compensation of gearless permanent magnet traction machine for direct-drive elevators," *IEEE Trans. Ind. Electron.*, vol. 61, no. 9, pp. 4594–4604, Sep. 2014.
[17] S. Kwak and J. C. Park, "Predictive control method with future zero-sequence voltage to reduce switching losses in three-phase voltage source inverters," *IEEE Trans. Power Electron.*, vol. 30, no. 3, pp. 1558–1566, Mar. 2015.
[18] T. Geyer and D. E. Quevedo, "Performance of multistep finite control set model predictive control for power electronics," *IEEE Trans. Power Electron.*, vol. 30, no. 3, pp. 1633–1644, Mar. 2015.
[19] Y. Cho, K. B. Lee, J. H. Song, and Y. I. Lee, "Torque-ripple minimization and fast dynamic scheme for torque predictive control of permanent-magnet synchronous motors," *IEEE Trans. Power Electron.*, vol. 30, no. 4, pp. 2182–2190, Apr. 2015.
[20] J. Han, S. K. Solanki, and J. Solanki, "Coordinated predictive control of a wind/battery microgrid system," *IEEE J. Emerging Sel. Topics Power Electron.*, vol. 1, no. 4, pp. 296–305, Dec. 2013.

[21] P. Karamanakos, P. Stolze, R. M. Kennel, S. Manias, and H. D. T. Mouton, "Variable switching point predictive torque control of induction machines," *IEEE J. Emerging Sel. Topics Power Electron.*, vol. 2, no. 2, pp. 285–295, Jun. 2014.
[22] B. Sun and Z. Gao, "A DSP-based active disturbance rejection control design for a 1-kW H-bridge DC–DC power converter," *IEEE Trans. Ind. Electron.*, vol. 52, no. 2, pp. 1271–1277, Oct. 2005.
[23] X. Chang, Y. Li, W. Zhang, N. Wang, and W. Xue, "Active disturbance rejection control for a flywheel energy storage system," *IEEE Trans. Ind. Electron.*, vol. 62, no. 2, pp. 991–1001, Feb. 2015.
[24] H. Sira-ramirez, J. Linares-Flores, C. Garcia-Rodriguez, and M. A. Contreras-Ordaz, "On the control of the permanent magnet synchronous motor: An active disturbance rejection control approach," *IEEE Trans. Control Syst. Technol.*, vol. 22, no. 5, pp. 2056–2063, Sep. 2014.
[25] D. Tian, H. Shen, and M. Dai, "Improving the rapidity of nonlinear tracking differentiator via feedforward," *IEEE Trans. Ind. Electron.*, vol. 61, no. 7, pp. 3736–3743, Aug. 2014.
[26] J. Wang, J. Zhang, and J. Yan, "A new second order nonlinear tracking differentiator and application," in *Proc. IEEE Int. Conf. Comput. Des. Appl.*, 2010, vol. 1, pp. V1–318–V1-322.
[27] P. Cortés, M. P. Kazmierkowski, R. M. Kennel, D. E. Quevedo, and J. Rodríguez, "Predictive control in power electronics and drives," *IEEE Trans. Ind. Electron.*, vol. 55, no. 12, pp. 4312–4324, Dec. 2008.
[28] M. Preindl and S. Bolognani, "Model predictive direct speed control with finite control set of PMSM drive systems," *IEEE Trans. Power Electron.*, vol. 28, no. 2, pp. 1007–1015, Feb. 2013.
[29] J. Q. Han, "From PID to active disturbance rejection control," *IEEE Trans. Ind. Electron.*, vol. 56, no. 3, pp. 900–906, Mar. 2009.

Gaolin Wang (M'13) received the B.S., M.S., and Ph.D. degrees in electrical engineering from the Harbin Institute of Technology, Harbin, China, in 2002, 2004, and 2008, respectively.

From 2009 to 2012, he was a Postdoctoral Fellow with Shanghai STEP Electric Corporation. In 2009, he joined the Department of Electrical Engineering, Harbin Institute of Technology, as a Lecturer, where since 2014, he has been a Professor of electrical engineering. He has authored more than 50 technical papers published in journals and conference proceedings. He is the holder of ten Chinese patents. His current major research interests include permanent magnet synchronous motor drives, high-performance direct-drive for traction system, position sensorless control of ac motors, and efficiency optimization control of interior PMSM.

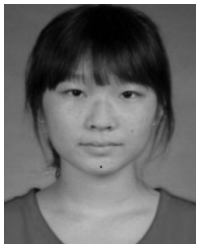

Ying Wang received the B.S. degree in electrical engineering from the Harbin Institute of Technology, Harbin, China, in 2014, where she is currently working toward the M.S. degree in power electronics and electrical drives at the School of Electrical Engineering and Automation.

Her current research interests include high-performance control strategy of permanent magnet traction system and position sensorless control.

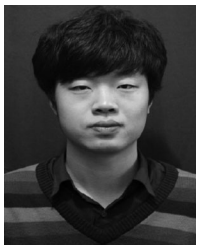

Jin Xu received the B.S. degree in electrical engineering from the Harbin Institute of Technology, Harbin, China, in 2013, where he is currently working toward the M.S. degree in power electronics and electrical drives at the School of Electrical Engineering and Automation.

His current research interests include direct-drive permanent magnet synchronous motor control and position sensorless control.

Nannan Zhao received the B.S. and M.S. degrees in control science and engineering from the Harbin Institute of Technology, Harbin, China, in 2013 and 2015, respectively, where he is currently working toward the Ph.D. degree in power electronics and electrical drives at the School of Electrical Engineering and Automation.

His current research interests include advanced control of permanent magnet synchronous motor drives and position sensorless control of ac motors.

Dianguo Xu (M'97–SM'12) received the B.S. degree in control engineering from Harbin Engineering University, Harbin, China, in 1982, and the M.S. and Ph.D. degrees in electrical engineering from the Harbin Institute of Technology (HIT), Harbin, in 1984 and 1989, respectively.

He was the Dean with the School of Electrical Engineering and Automation, HIT, from 2000 to 2010. In 1984, he joined the Department of Electrical Engineering, HIT, as an Assistant Professor, where since 1994, he has been a Professor, and currently the Vice President. He published more than 600 technical papers. His research interests include renewable energy generation technology, power quality mitigation, sensorless-vector-controlled motor drives, and high-performance servo system.

Dr. Xu is an Associate Editor of the IEEE TRANSACTIONS ON INDUSTRIAL ELECTRONICS and the IEEE JOURNAL OF EMERGING AND SELECTED TOPICS IN POWER ELECTRONICS. He serves as the Chairman of the IEEE Harbin Section.